Forestry An International Journal of Forest Research

Institute of Chartered Foresters

Forestry 2015; **88**, 429–440, doi:10.1093/forestry/cpv012
Advance Access publication 21 May 2015

A novel method to assess short-term forest cover changes based on digital surface models from image-based point clouds

Zuyuan Wang*, Christian Ginzler and Lars T. Waser

Department Landscape Dynamics, Swiss Federal Research Institute WSL, Zuercherstr. 111, CH-8903 Birmensdorf, Switzerland

*Corresponding author. Tel: +41 447392691; Fax: +41 447392215; E-mail: zuyuan.wang@wsl.ch

Received 31 July 2014

Assessing forest cover change is a key issue for any national forest inventory. This was tested in two study areas in Switzerland on the basis of stereo airborne digital sensor (ADS) images and advanced digital surface model (DSM) generation techniques based on image point clouds. In the present study, an adaptive multi-scale approach to detect forest cover change with high spatial and temporal resolution was applied to two study areas in Switzerland. The challenge of this approach is to minimize DSM height uncertainties that may affect the accuracy of the forest cover change results. The approach consisted of two steps. In the first step, a 'change index' parameter indicated the overall change status at a coarser scale. The tendency towards change was indicated by derivative analysis of the normalized histograms of the difference between the two canopy height models (DCHMs) in different years. In the second step, detection of forest cover change at a refined scale was based on an automatic threshold and a moving window technique. Promising results were obtained and reveal that real forest cover changes can be distinguished from non-changes with a high degree of accuracy in managed mixed forests. Results had a lower accuracy for forests located on steep alpine terrain. A major benefit of the proposed method is that the magnitude of forest cover change of any specific region can be made available within a short time as often required by forest managers or policy-makers, especially after unexpected natural disturbances.

Introduction

Assessing forest cover change is an important task because it is a fundamental input for a broad range of applications, such as planning afforestation or development in order to preserve forest ecosystem balance. Thus, one of the major tasks of national forest inventories (NFIs) is to estimate forest resources and assess changes in order to support sustainable management.

Nowadays, most NFIs are sample-based terrestrial inventories with an efficient integration of different information sources including remote sensing. Remote sensing in particular provides the data required for the most meaningful and commonly reported NFI parameters, such as growing stock, forest area and forest land use change (Lawrence *et al*., 2010). Moreover, remote sensing data have contributed to the optimization of field work and the reduction of estimation error for these inventory parameters (McRoberts and Tomppo, 2007; Maltamo *et al*., 2014).

In contrast, assessing changes in forest parameters using NFI plot data is a highly complex and challenging task since it depends on the sampling design and time span between each inventory cycle. For example, the sampling design of the Swiss NFI is a continuous survey where one-ninth of all plots are assessed each year. Although the plots visited in any 1 year are evenly distributed over the country and change can be estimated at an annual scale, the estimation error is very high and is larger for smaller areas with fewer plots. Thus, estimating changes over a short-time period based on NFI plot data remains a challenging task.

Multispectral and high spatial resolution remote sensing data offer the possibility of extending the spatially and temporarily limited NFI plot information to a continuous landscape-level representation, such as wall-to-wall products. Moreover, due to the recent improvement in the quality of multispatial and multitemporal remote sensing data, together with advanced image processing algorithms, several studies have shown that it is now feasible to detect forest cover changes in a timely and cost-effective manner. Initially, assessing forest cover change was done through visual interpretation of aerial (Spurr, 1960; Paine and Kiser, 2003) or satellite imagery (Bauer *et al*., 1994). In recent years, numerous approaches to detect forest cover change based on different scales and sensors have been developed. Fraser *et al*. (2005), for example, assessed forest cover change over large areas based on low spatial resolution SPOT VEGETATION and NOAA AVHRR imagery. Song *et al*. (2014) used a time series from the Moderate Resolution Imaging Spectroradiometer (MODIS). Hayes and Cohen (2007) used a combination of MODIS and Landsat imagery. Medium spatial resolution sensors have also been used. Examples include imagery from SPOT used by Desclée *et al*. (2006), Landsat used by Baumann *et al*. (2012), a combination of ASTER, SPOT-4 and Landsat-5 used by Wulder *et al*. (2008) and Hansen *et al*. (2013) who used Landsat time series to generate a global map of forest cover change. Change detection analysis was carried out by Elhadi and Zomrawi (2009) based on high-resolution Ikonos and Quickbird imagery and based on aerial imagery by Baker *et al*. (1995) and Waser *et al*.

(2008). However, increasing spatial resolution is also considered to be one of the sources of uncertainty in change detection because of the effects of geo-referencing, higher spectral variability and acquisition characteristics (Hussain *et al.*, 2013). A review of methods for assessing uncertainty and accuracy of land cover change can be found in Olofsson *et al.* (2014).

According to Dai and Khorram (1999), change detection using multispectral images can be based on either post-classification comparison or direct change detection algorithms. These state-of-the-art remote sensing change detection methods have been extensively reviewed, and the relative strengths and weakness of these approaches are well reported in the literature (Singh, 1989; Mas, 1999; Coppin *et al.*, 2004; Lu *et al.*, 2004; Wulder *et al.*, 2008).

Nowadays, with the availability of accurate 3D data, changes in forest parameters can be assessed by detecting changes in the surface elevation of the canopy cover using digital surface models (DSMs) from different dates. DSMs derived from airborne laser scanning (ALS) have been used to estimate canopy attribute changes (Wulder *et al.*, 2007) or to assess changes in above-ground biomass (Skowronski *et al.*, 2014). DSMs derived from image-matching-based point clouds have also been used to assess changes in forest cover (Waser *et al.*, 2008; Tian *et al.*, 2013).

As stated by Straub *et al.* (2013), current technical advances in the field of digital photogrammetry demonstrate the great potential of automatic image matching to derive dense surface models for forest canopies. This renewed interest in using digital image matching has occurred because of the improved radiometry of digital images (e.g. 16-bit data), the simultaneous use of multiple images (Zhang and Gruen, 2006) and new algorithmic solutions, such as semi-global matching (Hirschmüller, 2008), as well as improvements in commercial matching software (Haala, 2009).

In contrast to ALS, digital aerial stereo images are updated more regularly by national or regional mapping agencies in several countries. Thus, new possibilities for assessing forest cover changes are provided by frequently updated DSMs over entire countries (Ginzler and Hobi, 2015). This is the case in Switzerland, where the Federal Office of Topography (swisstopo) has updated the country-wide digital stereo imagery every 3 years since 2008. As a result, assessing forest cover change with high spatial and temporal resolution might be feasible for one-third of the country every year. Nonetheless, there is currently little experience in assessing forest cover changes under these specific conditions. An extended assessment of forest cover change from small areas of a few square kilometres (Waser *et al.*, 2008; Tian *et al.*, 2013) to larger areas or entire countries will become more feasible in the near future.

According to White *et al.* (2013), general factors affecting the quality and completeness of DSMs may include the resolution and overlap of images, occlusions and excessive image displacement in areas of tall trees as off-nadir angle increases. For multi-temporal images, differences in image orientation as well as sun elevation angles also have an impact on the quality of generated DSMs. For example, the difference between the azimuths of the sensor and the sun usually leads to a shadow in non-occluded areas, consequently having a significant impact on the generated DSMs. If one of these two generated DSMs contains any artefacts introduced by such factors, simple subtraction would result in a combination of real and virtual changes. Therefore, the greatest remaining challenge of the proposed method was to separate virtual changes from real changes in a robust and effective manner.

The objective of the present study was to assess forest cover change in two study areas in Switzerland on the basis of stereo airborne digital sensor80 (ADS80) images. To achieve optimal results, a novel adaptive multi-scale approach was developed to capture real changes. Changes were detected from scales ranging from coarser to refined based on a hierarchical strategy. Because there is a 3-year difference between the images, the forest cover change under examination was the 'lost' (or 'eliminated') part. The results open new possibilities to complement the tasks of the Swiss NFI, including the detection of area-wide forest cover change and areas with no change, which are both essential for planning and management purposes in managed forests in flatlands. The potential and the limits of the proposed method were also discussed, in particular, regarding the challenging topography in mountainous areas.

Materials and methods

Study area

Assessing changes in the forest cover was tested in two study areas with contrasting topography, forest structure, condition and management. Each had an approximate size of 17.5 × 11.5 km (Figure 1). Study area 1 is located in the Central Swiss Plateau (8° 16′ E, 47° 22′ N) with an elevation ranging from 350 to 800 m above sea level (a.s.l.). 43 per cent of the area is agricultural, whereas 32 per cent is mostly managed mixed deciduous and coniferous forests, 23 per cent settlements and 2 per cent unproductive areas. The entire area belongs to one of the most productive areas in Switzerland in terms of wood production. The most dominant tree species are beech (*Fagus sylvatica* L.), ash (*Fraxinus excelsior* L.), oak (*Quercus sp*), white fir *(Abies alba* Mill.) and Norway spruce (*Picea abies* L.).

Study area 2 is located in the Central Alps of the Valais (7° 34′ E, 46° 18′ N) with an elevation ranging from 500 to 2900 m a.s.l. and an upper tree line at ∼2200–2300 m a.s.l., 45 per cent of the area is forested, 27 per cent agricultural, 12 per cent settlements and 16 per cent unproductive areas. The forests are managed and have a high protection function. The most dominant tree species are Scots pine (*Pinus sylvestris* L.), larch (*Larix deciduas* Mill.) and Norway spruce (*Picea abies* L.) in addition to a few deciduous tree species and softwood species along the Rhone river in the valley.

Remote sensing data

Since 2008, swisstopo has acquired stereo image data from the Airborne Digital Sensors ADS40-SH52 and ADS80-SH82 (Sandau *et al.*, 2000) for the entire country on a 3-year cycle. Consequently, one-third of Switzerland is updated every year with ADS imagery with a spatial resolution of 25 or 50 cm. All images of study area 1 have a spatial resolution of 25 cm. In study area 2, 70 per cent images have a spatial resolution of 25 cm and the rest 50 cm. Stereo image pairs taken from ADS80 sensors are used as input data for country-wide DSM generation (Bühler *et al.*, 2012).

To minimize any impact on the corresponding DSMs (such as the notable differences that can be clearly seen between DSMs derived from leaf-on and leaf-off images), the selection of appropriate imagery from 2010 and 2013 was restricted to the date of image acquisition (preferably from the leaf-on season). In the present study, images were acquired during the vegetation seasons (from June to September).

The data including the absolute orientation of the images were provided by swisstopo. The residuals of the absolute orientation are reported to be +/−1 pixel (swisstopo, 2015). The sensor collects multispectral images (blue, green, red and near infra-red) at two viewing angles (nadir and 16° backward) simultaneously, and the radiometric resolution of the images is 12-bit. Tables 1 and 2 show the image data information acquired in

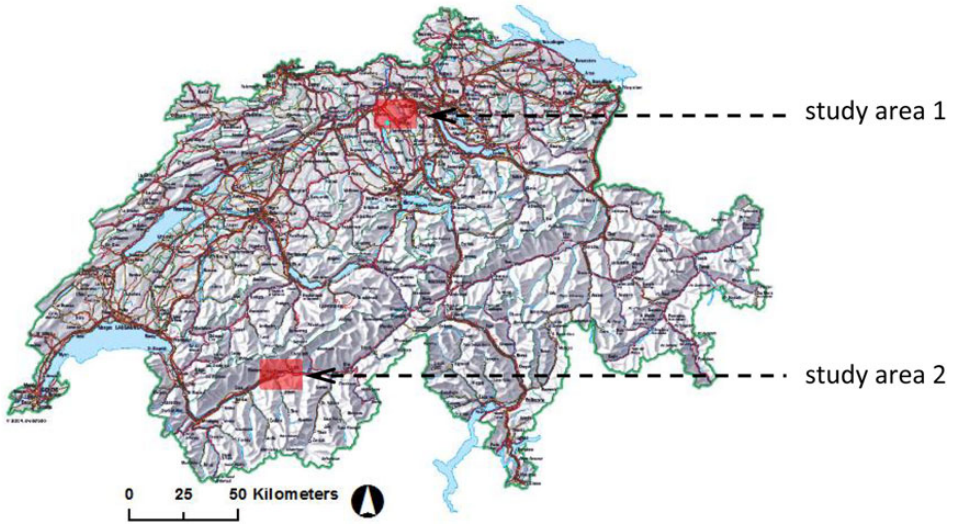

Figure 1 Location of the two study areas (highlighted boxes).

Table 1 Image data information acquired in 2010 for the two study areas

	Study area 1	Study area 2
Sensor type	ADS80-SH82	ADS80-SH82
Number of stripes with ground sample distance of 25 cm	8	7
Number of stripes with ground sample distance of 50 cm		5
Acquisition date(s)	June 05, June 24, July 07	May 23, May 24, August 09, August 22
Orientation accuracy	±1 GSD	±1 GSD

Table 2 Image data information acquired in 2013 for the two study areas

	Study area 1	Study area 2
Sensor type	ADS80-SH82	ADS80-SH82
Number of stripes with ground sample distance of 25 cm	8	17
Number of stripes with ground sample distance of 50 cm		4
Acquisition date(s)	June 13, June 17	July 31, August 01, August 10, August 15, September 03, September 04
Orientation accuracy	±1 GSD	±1 GSD

2010 and 2013, respectively. A more detailed description of these image data can be found in Waser *et al.* (2011).

In the first step, two DSMs with a spatial resolution of 1 m were calculated from the false-colour infra-red (FCIR) images with the colour composite near infra-red, red and green bands using the 'Next Generation Automatic Terrain Extraction' (NGATE) (Zhang *et al.*, 2007). This algorithm was provided by the commercially available photogrammetric software SocetSet (BAE Systems). To manage high texture and small-scale elevation changes (e.g. open forests) and homogenous areas with little texture (e.g. meadows), two different matching strategies were used, both based on image correlation and edge matching (Ginzler and Hobi, 2015). In the second step, two canopy height models (CHM) were calculated by subtracting the digital terrain model (DTM) from the DSMs. The DTM 'swissALTI3D' is the product of the national light detection and ranging campaign and was provided by swisstopo (Artuso *et al.*, 2003). The 1-m DSMs and DTM served as a basis for all investigations of this study.

Automatic forest cover change detection based on multi-scale analysis

A two-step procedure, from a coarser-scale to a refined-scale, was implemented to automatically detect forest cover change. Figure 2 shows the workflow of detecting the 'change'. In the first step, a difference between

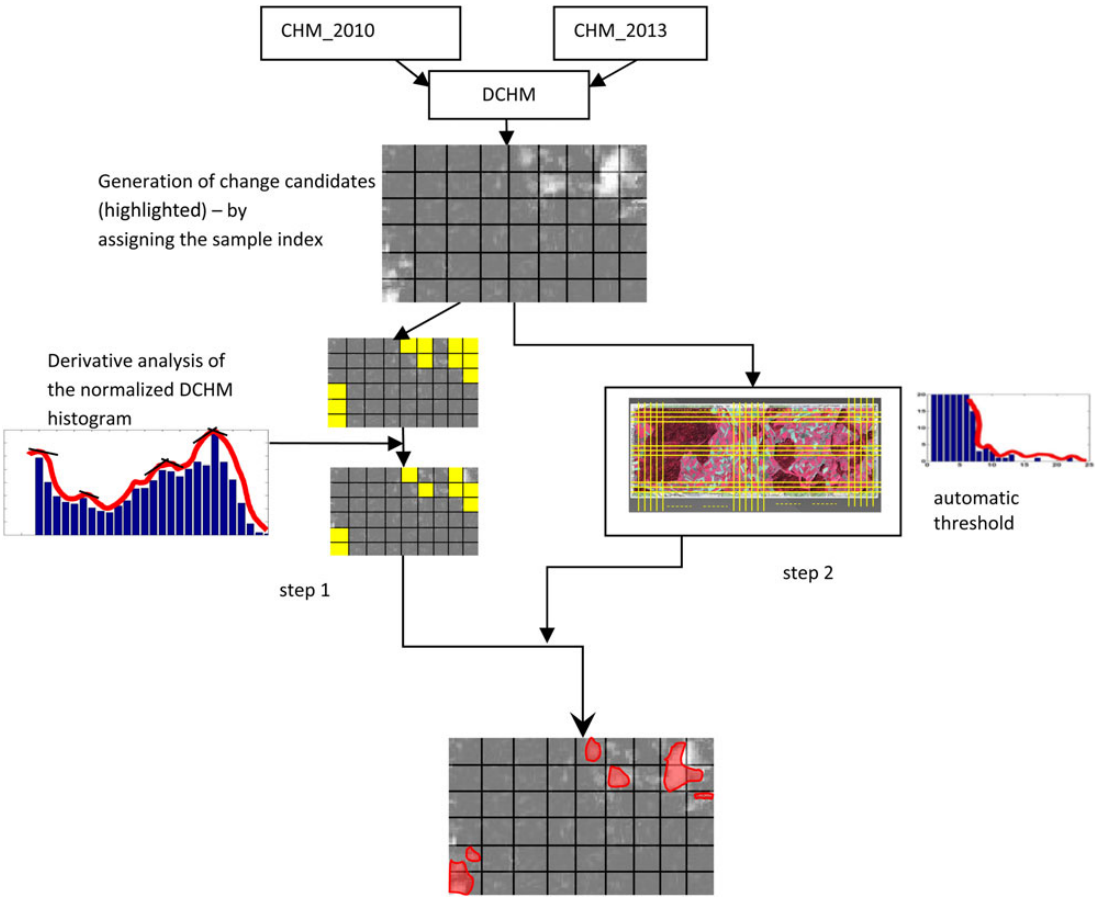

Figure 2 Workflow of the forest cover change approach.

the two canopy height models (DCHMs) was computed by subtracting the CHM_2010 from the CHM_2013. In this first step, the changes in the DCHMs were looked for at the coarser-scale (50 × 50 m), which corresponds to the plot size of the Swiss NFI. This step also included the assignment of the sample index and the derivative analysis of the normalized DCHM histogram. In the second step, a pixel-wise fine-scale detection was performed with an automatic threshold by zooming into the blocks with changes that were detected at the coarser-scale (Figure 3). Detailed information is given in the following sections.

Assigning the sample index

According to the definition of the Swiss NFI, the height of a tree should be at least 3 m. If a tree was lost/eliminated, the 'sign change' would be given when the difference shown in the DCHMs was at least 3 m. Therefore, for each 50 × 50 m block, the pixels that had the 'sign changes' were counted. The total number of pixels with the 'sign changes' was named as 'num_change'. For all the pixels with the 'sign changes', their DCHM values were taken into account and sum them up to a number, namely, 'sum_change'. Thus, an average value ('avg_change') among these pixels with the 'sign changes' could be defined:

$$\text{avg\_change} = \text{sum\_change}/\text{num\_change}. \quad (1)$$

Next, the proportion of the pixels with the 'sign changes' in each block was required. 'Window size' was defined as the total number of pixels in the block. The proportion ('change_ratio') was calculated thus:

$$\text{change\_ratio} = \text{num\_change}/\text{window\_size}. \quad (2)$$

If an average value (of all the differences in this block) for all the pixels in the block was calculated, a 'change index' was obtained:

$$\text{change\_index} = \text{sum\_change}/\text{window\_size} = \text{change\_ratio} \times \text{avg\_change}. \quad (3)$$

If the 'change index' was larger than an empirical threshold th_{index}, a sample index '1' was assigned to this block. Otherwise, the sample index '0' was assigned.

Derivative analysis of the normalized DCHM histogram

In order to determine the tendency towards change that occurred within a 50 × 50 m block, a general histogram was produced as follows. First, the differences indicated by the DCHMs were classified into 5-m-range classes, such as (<5), (5 to <10), (10 to <15 m) and so on. Then, a frequency histogram was built. Finally, the total number of pixels was normalized by the total pixels (2500) in this block, as described in the formula:

$$n = \sum_{i=k}^{k+1} m_i/(\text{window\_size}) \quad k = 0,\ 1,\ 2 \ldots 7 \quad (4)$$

where m_i was the total number of pixels in a specific block ($[k\ k+1) \times 5$ m) and n was a normalized histogram.

If the envelope curve of the histogram decreased monotonically, the differences were interpreted as noise or salt-and-pepper effect and implied that no change had occurred. Otherwise, the curve would show jumps at some classes. The derivative of the envelope curve of the histogram was

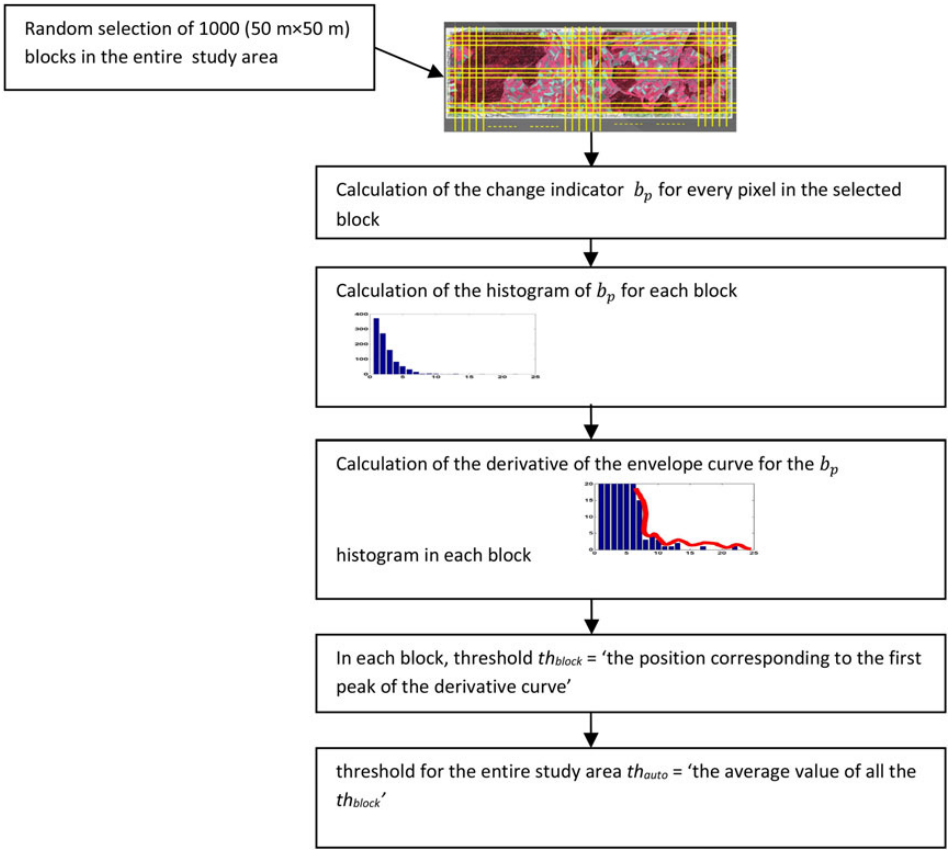

Figure 3 Automatic threshold algorithm.

used to determine whether its tendency followed a monotonic decrease. In the present study, for an obtained histogram, the first derivative of its envelope curve was calculated. If the obtained derivatives in any place were greater than 0, a relevant big change had occurred.

If no 'big change' in a class width of 5 m was indicated, the class width was reduced to 2 m, and the entire process redone. In this case, if the derivative was >0, a 'small change' was detected in this block. If the block had either a 'small change' or a 'big change', the block would be catalogued as an area that had undergone change at the coarser-scale.

Refined-scale detection and automatic threshold selection

With the coarser-scale detection, coarse change areas could be identified. Nevertheless, inside those areas, it was still necessary to carry out the refined-scale detection at the pixel level to determine the forest cover change precisely. In order to avoid salt-and-pepper effects in the DCHM data, for each pixel (highlighted point in Figure 4) in the 50 × 50 m block where a coarse change had been indicated, the mean value of the DCHMs using a moving window was calculated. The used size was empirically tested by applying an 11 × 11 m window which corresponds to a typical relatively large tree crown size. Comparing this mean value with the automatic selected threshold (explained below), each pixel could be distinguished as 'change' or 'non-change'.

For the refined-scale detection, the key issue was to set a threshold. Regarding DSM data uncertainty, the selection of thresholds should be reasonable and robust. The proposed method to select the threshold automatically is described as follows:

(1) In the whole study area, one thousand 50 × 50 m blocks were randomly selected in the CHM_2010 grid map.

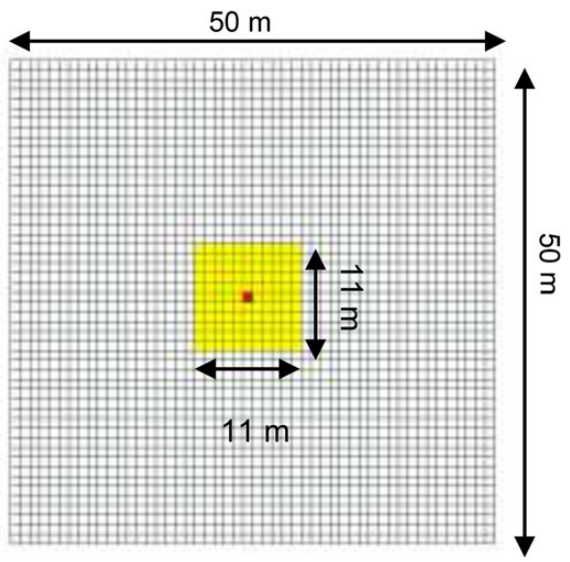

Figure 4 An 11 × 11 m moving window centred by each pixel, within a 50 × 50 m image block.

(2) For every pixel in a block, a window (11 × 11 m) centred by this pixel was generated. Hereafter, each pixel in this window ('window pixel') was examined by the following tree definition. If the window_pixel with the value given by the CHM_2010 was not <3 m, a 'tree index' would be assigned to the window_pixel, and its CHM value was recorded as

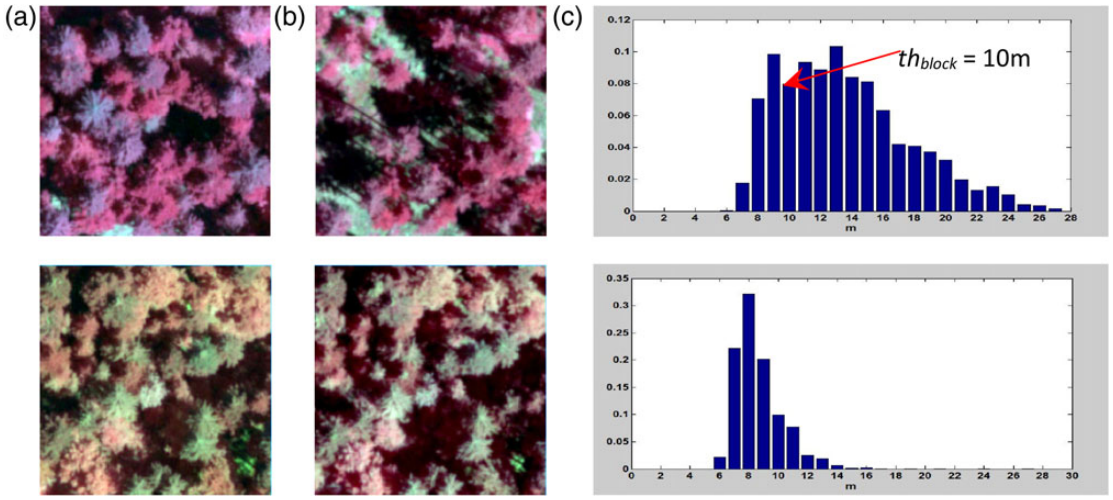

Figure 5 b_p histogram and automatic threshold selection. From top to bottom, each row denotes one block image. (a) FCIR taken in 2010, (b) FCIR taken in 2013, (c) b_p histogram and its corresponding th_{block}.

'value_tree_2010'. For the same window_pixel, the value given in the CHM_2013 was recorded as 'value_tree_2013'. The difference ('delta_height') between 'value_tree_2013' and 'value_tree_2010' was calculated for the window_pixel thus:

$$\text{delta\_height} = \text{abs}(\text{value\_tree\_2013} - \text{value\_tree\_2010}). \quad (5)$$

For the entire window, the number of window_pixels with 'tree index' in CHM_2010 was counted ('sum_tree_pixel'). Correspondingly, their 'delta_height' values were added up ('sum_delta_height'). The parameter used to measure the degree of change in tree heights from 2010 to 2013 inside this window was calculated by:

$$b_p = \frac{\text{sum\_delta\_height}}{\text{sum\_tree\_pixel}}. \quad (6)$$

Obviously, every pixel in the block would have an indicator, 'b_p', namely 'change_variation', to express the change. This indicator measured the degree of change by considering possible inconsistency using the image-matching method to generate DSMs at different dates. The window with sum_tree_pixel =0 was ruled out. Naturally, the specified pixel in the block was ruled out as well.

(3) For each block, all the pixels in the block and their corresponding 'b_p' values were obtained. Again, a histogram of the 'b_p' values in 1-m classes was produced. The derivative of the envelope curve of the histogram was calculated. The position corresponding to the first peak of the derivative curve (meaning that a significant 'change' had happened) was defined as the threshold 'th_{block}'. Figure 5 shows an example of b_p histograms for two blocks, where there were changes in Block 1 and no changes in Block 2. It was worth mentioning that a block was ruled out if the derivative curve was smooth and had no peaks.

Accuracy assessment

As reference data, 50 × 50 m squares were visually checked and interpreted as to whether a change or non-change in the forest cover occurred in the corresponding images between 2010 and 2013. Only NFI plots that were coded as forest were used as reference data (Figure 6). A total of 263 plots in study area 1 and 838 plots in study area 2 were marked as forests in the NFI. Overall, forest cover change was detected in 16 per cent of the reference squares in study area 1 and 2 per cent in study area 2.

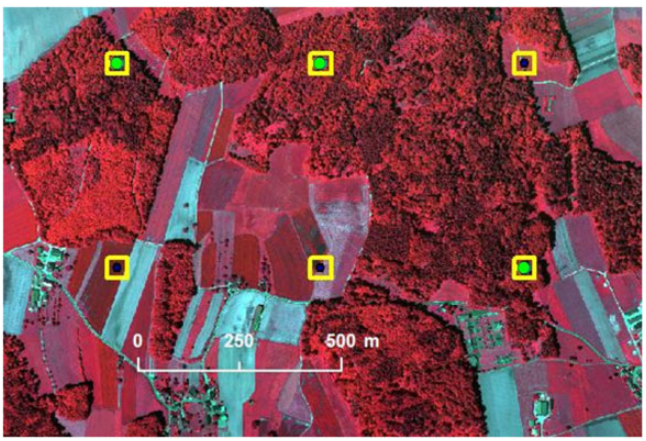

Figure 6 Manual interpretation areas for change/non-change decision on the sample plot area defined as forest in Swiss NFI. (a 50 × 50 m sample plot area defined as 'forest', a 50 × 50 m sample plot area defined as 'non-forest').

Results

Automatic detection of forest cover change

Following the workflow illustrated in Figure 2, the automatic change detection was performed on the study area as presented in Figure 1. Here, the threshold for 'change index' was empirically determined as th_{index} =1.3. In addition, the automatic threshold th_{auto} generated from 1000 randomly selected blocks was calculated to be 10.26 m for study area 1 and 8.5 m for study area 2. The final result is shown in Figure 7, where the detected changes are highlighted. In Figure 8, two zoomed-in areas in both study areas are shown, where the circles indicate where significant changes had occurred. In order to test forest cover

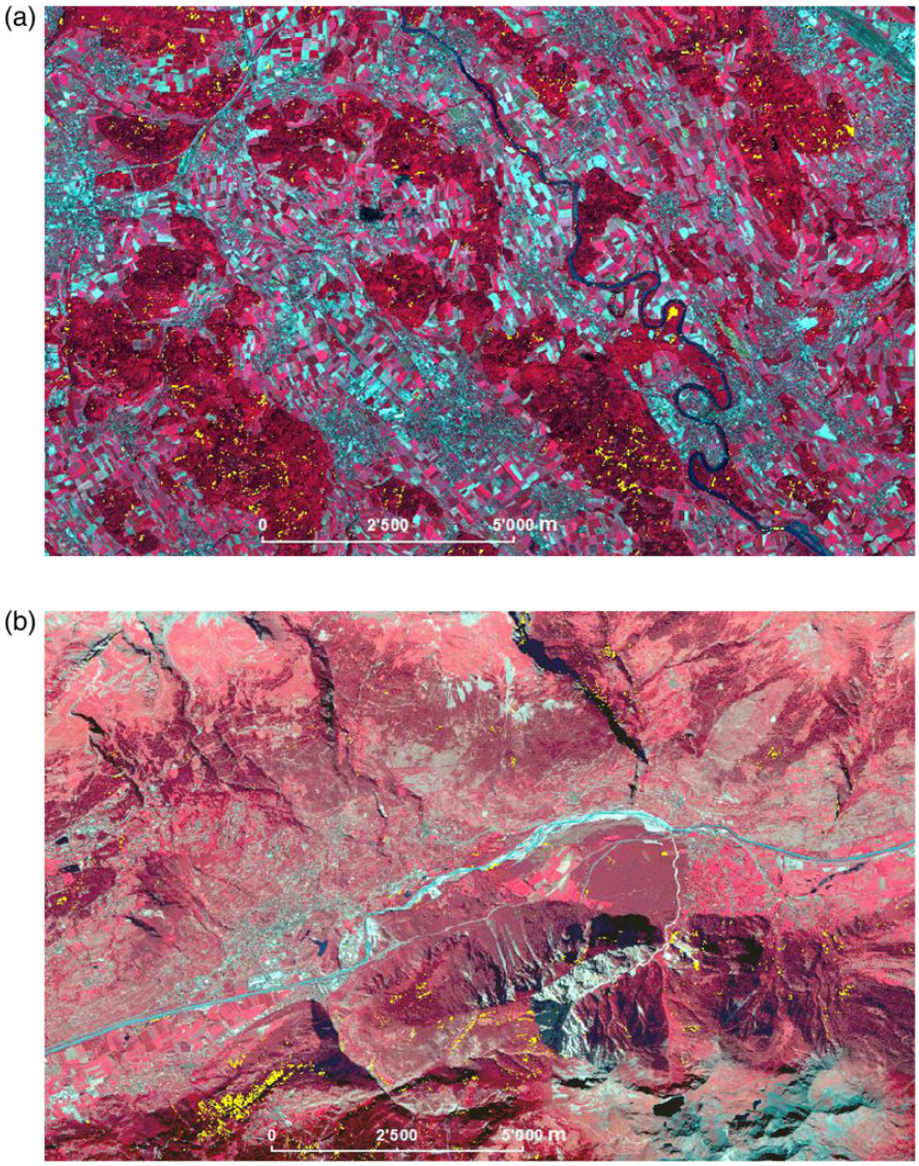

Figure 7 Change detection result. (a) Study area 1, (b) study area 2 (forest cover changes highlighted on FCIR acquired in 2010).

change accuracy with different thresholds in study area 1, two experiments where th_{auto} was set manually to 5 and 15 m were conducted.

DSMs quality analysis

Figure 9 illustrates forest cover change and non-change in three profiles. The profiles in Figures 9a (forest area) and 9b (non-forest area) show no forest cover changes. As a comparison, Figure 9c illustrates the profile of an area with forest cover changes. It should be noted that in forest areas, there are more artefacts in the DSMs generated from the stereo imagery than in other non-forest area.

Figure 10a and b shows the FCIR images acquired in 2010 and 2013 for the same area, with the corresponding CHMs (Figure 10d and e) and the DCHM values of larger than th_{auto} (highlighted areas in Figure 10c). The result implied that the forest cover has changed. However, visual inspections revealed that forest cover had not changed in this area. Obviously, the uncertainty of the generated data sets introduced errors into the forest cover change result.

Accuracy assessment

In summary, the overall accuracy was 93 per cent for study area 1 with the proposed method, 85 per cent when th_{auto} was set to 5 m and 93 per cent when th_{auto} was set to 15 m. The overall accuracy for study area 2 was higher, with 98 per cent. The accuracy assessments for the proposed method in study areas 1 and 2 and those of two different assigned threshold experiments in study area 1 are shown in Table 3.

Examples of forest cover change in study area 2

The producer's accuracy and user's accuracy of forest cover change detection in study area 2 were relatively low. In fact, real changes

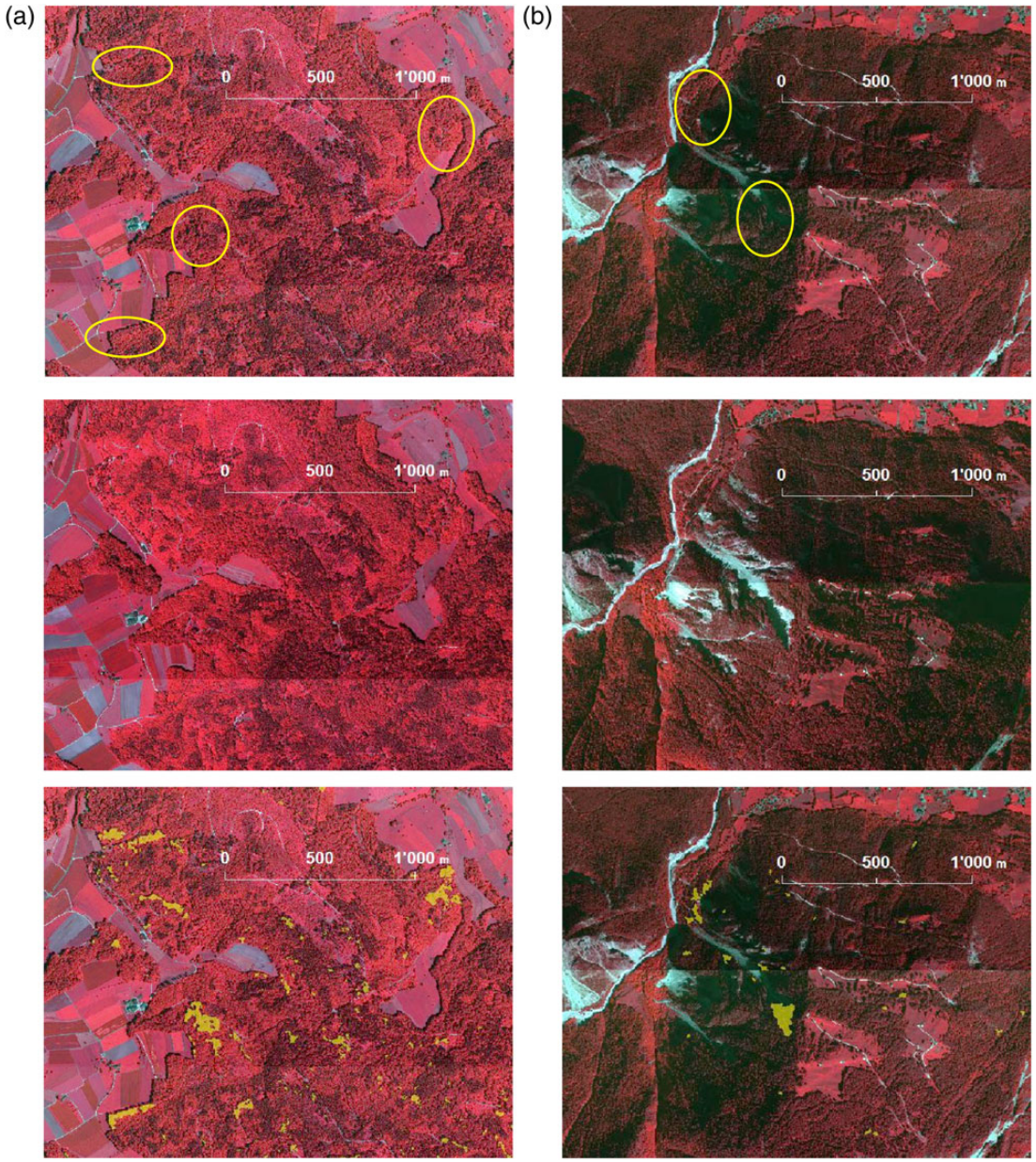

Figure 8 Detection of forest cover change in zoom-in areas. (a) Study area 1, (b) study area 2. From top to bottom: (1) FCIR taken in 2010, circles indicate significant changes, (2) FCIR acquired in 2013, (3) areas with forest cover change (highlighted) on FCIR acquired in 2010.

were successfully detected by the proposed method. However, these changes were not taken into account since the reference data were based on the interpreted squares following the Swiss NFI sample plots. Figure 11 shows the final forest cover as a result of the steep terrain in this alpine region. Figure 12 illustrates the erroneous forest cover change detection due to large shadows in the 2010 images.

Discussion and conclusion

In the present study, a novel adaptive multi-scale approach was developed, which enables the detection of forest cover change and the ability to distinguish between real changes and non-changes with high overall accuracy. The results indicate that the method is promising and provides a high degree of accuracy in managed mixed forests, with lower accuracies in mountainous forests. These results suggest that the proposed method can provide essential and valuable information on the magnitude of change/non-change in forest cover as needed for proper forest management. The proposed approach makes it possible to map forest cover changes at a 1 m spatial resolution which can be used operationally at a regional and national scale as complementary data to Swiss NFI surveys.

A significant challenge for this approach was to minimize uncertainties regarding height information in the CHMs, which impact

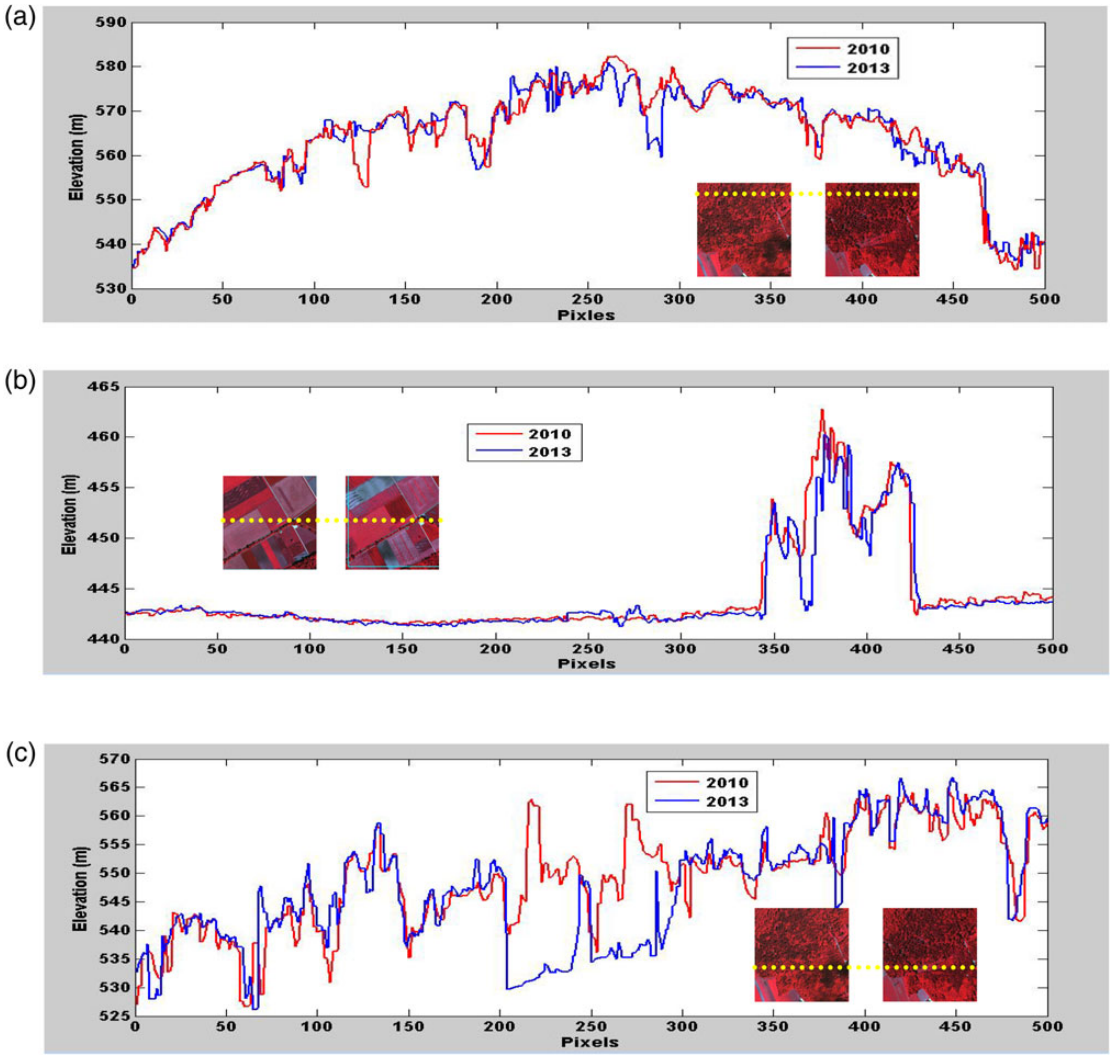

Figure 9 DSM analysis of different land covers. Image pairs in each row: on the left acquired in 2010; on the right, in 2013. The dotted line indicates the profile position. In each graph, the lines show the profiles in the 2010 and 2013 imagery separately. From top to bottom: (a) forest cover area without change, (b) non-forest area without change and (c) forest cover area with change.

results by detecting erroneous changes. Using a threshold based on some prior knowledge enabled the identification of areas with erroneous height changes using a 'change index'. Derivative analysis of the normalized DCHM histograms, which tracked the tendency to change in each block, facilitated more accurate location of real changes. In this step, areas with erroneous changes were removed, resulting in substantially improved change detection accuracy. The proposed automatic threshold selection for the refined-scale change detection made the method more robust in comparison with using a predefined threshold.

The proposed indicator 'change_variation' b_p measured the amount of change around each pixel by taking DCHM variations in a moving window into account. The b_p histogram of each coarser block characterizes the change trend. Thus, the correct localization of change is indicated by the location of the first peak of the envelope curve of the b_p histogram.

Both producer's accuracy (83 per cent) and user's accuracy (76 per cent) for study area 1 were good. The method detected 11 sample plots that were defined as 'non-change' in the reference data set. This was mainly accounted for by the difference between the calculated DSMs affected by shadows in the forests.

Although study area 2 is a mountainous area, where naturally caused forest cover change hazard events were expected, only a few such forest cover changes were detected between 2010 and 2013. Therefore, there were only a small number of plot areas referenced as changes. For the proposed method, both producer's (53 per cent) and user's accuracies (42 per cent) were substantially lower. At this point, it should be noted that visual image interpretation revealed that forest cover changes were detected mostly outside of the NFI plot data. Thus, future work should enlarge reference data sets, for example, by testing it in areas with a denser distribution of NFI plots.

In both study areas, producer's accuracies were higher than user's accuracies. This was the result of detecting more non-change areas referenced as change areas in comparison with change areas referenced as non-change areas. There are multiple

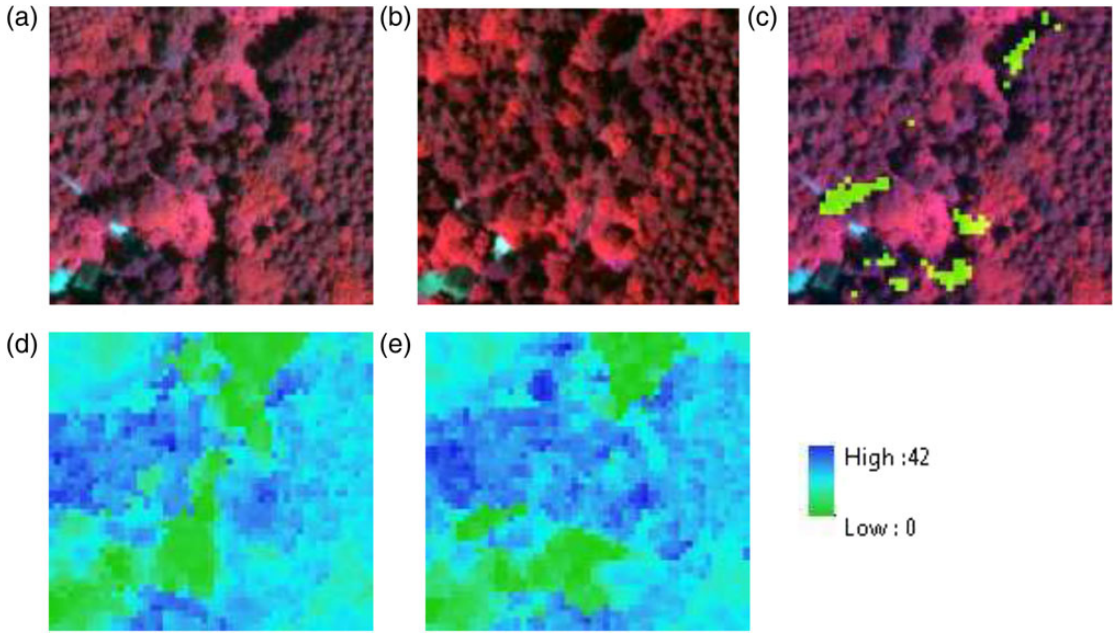

Figure 10 FCIR images, corresponding DSMs and DCHMs of the same area. (a) FCIR acquired in 2010, (b) FCIR acquired in 2013, (c) calculated DCHMs, with DCHMs $> th_{auto}$ (highlighted) on FCIR 2010, (d) CHM in 2010 and (e) CHM in 2013.

Table 3 Accuracy assessment for study areas 1 and 2

	Producer's accuracy (change)	User's accuracy (change)	Producer's accuracy (non-change)	User's accuracy (non-change)	kappa	Overall accuracy
Study area 1						
Proposed method	0.83	0.76	0.95	0.97	0.75	0.93
Threshold (=15 m)	0.62	0.90	0.99	0.93	0.69	0.93
Threshold (=5 m)	0.86	0.51	0.85	0.97	0.55	0.85
Study area 2						
Proposed method	0.53	0.42	0.99	0.99	0.46	0.98

reasons for this. The first reason is related to the generation of DSMs and DCHMs, which was affected by different sun elevations between image acquisitions, which produced shadows in 2010 images and no shadows in 2013 images or vice versa. Since the used images were acquired by swisstopo in the framework of national flight campaigns, controlling over the date and time of image acquisition was impossible, and thus, some shadows had to be accepted. Consequently, in future work, shadows will be identified using spectral information and can be, thus, treated separately in the change detection algorithm and excluded from the analysis.

The second reason is related to the oblique problem between the generated DSMs as a result of different flight angles of the imagery acquired in 2010 and 2013. This is an important issue regarding the lower accuracies in mountainous areas, i.e., study area 2. Comparisons between Figures 9 and 10 indicate that some differences, as a result of displacement, may occur between the DSMs of different dates. Moreover, DSM quality is affected by many factors. For example, if the flight path is not identical on the two image acquisition dates, the objects in the images have different distances to the nadir lines. In this particular case, the relief displacement due to the height of the objects will exist in the generated DSMs and cannot be ignored. For example, Poon *et al.* (2005) and Hobi and Ginzler (2012) stated that the accuracy of a DSM within the forest area is lower than that is for other land cover types (e.g. flat terrain, herbs and grass, pastures, etc.). Another area worth exploring is the testing of novel image-matching algorithms to further improve the accuracy of the generated DSMs as suggested in Mortensen *et al.* (2005); Choi and Kweon (2009) and Tack *et al.* (2012).

To summarize, the present study has demonstrated that because of the benefits of increasingly advanced techniques in the generation of image-based point clouds, the proposed approach enables the assessment of forest cover changes with a high degree of automation for large areas, even at the national scale. Thus, the main contribution of this study to the field has been to test the robustness of the method and its suitability in providing complementary information to the Swiss NFI. With the proposed approach, real forest cover changes can be detected and distinguished from virtual changes. The method was based on a

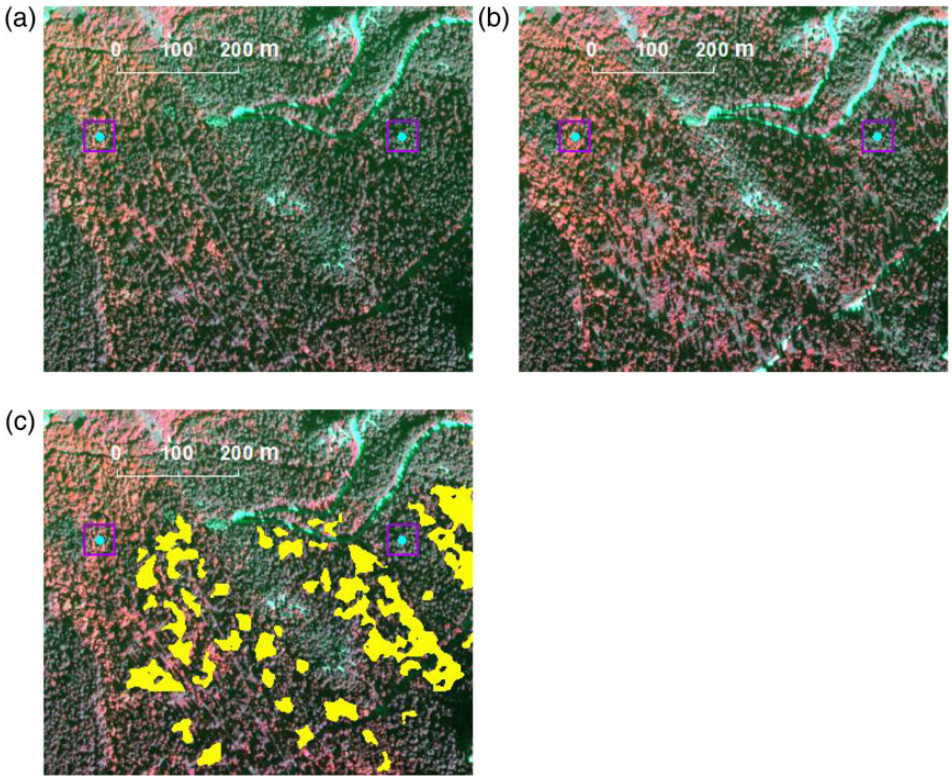

Figure 11 Example of erroneous forest cover change outside the 50 × 50 m NFI sample plot area (square). (a) FCIR 2010 image, (b) FCIR 2013 image and (c) detected forest cover changes (highlighted) on the 2010 FCIR image.

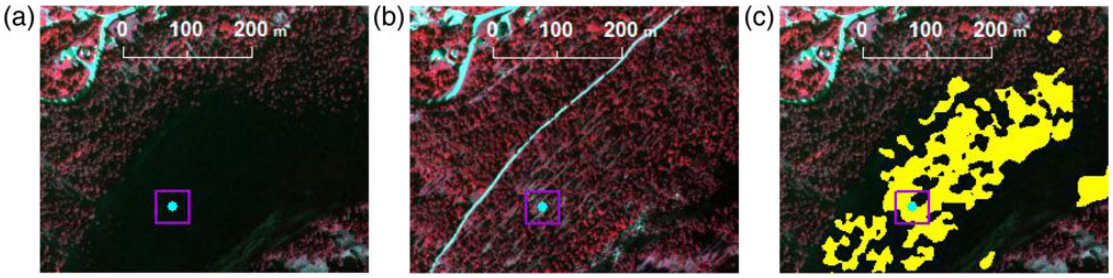

Figure 12 Erroneous forest cover change due to large shadows in mountainous study area 2, where the square indicates the NFI 50 × 50 m sample plot area. (a) FCIR in 2010, (b) FCIR in 2013 and (c) detected forest cover changes (highlighted) on FCIR in 2010.

multi-scale analysis from coarser to refined change detection, which is well-suited for VHR data sets. It is flexible and fast since it does not require any initial training. The study also demonstrates that height information can be a reliable source for the gathering of change information by minimizing false positive forest cover changes. Moreover, up-to-date and accurate information on forest cover changes after natural and anthropogenetic disturbances, such as fire, storms or avalanches, can be provided within a short time.

Acknowledgements

We thank the two anonymous reviewers for their valuable comments and suggestions to improve the manuscript. We also thank Curtis Gautschi for the professional language editing.

Conflict of interest statement

None declared.

Funding

This study was funded by the Swiss National Forest Inventory (NFI), a co-operation between the Swiss Federal Research Institute WSL and the Swiss Federal Office for the Environment FOEN.

References

Artuso, R., Bovet, S. and Streilein, A. 2003 Practical methods for the verification of countrywide terrain and surface models. In *ISPRS working group III/3 workshop XXXIV-3/W13. 3-D reconstruction from airborne laserscanner and InSAR data* Dresden, Germany.

Baker, W.L., Honaker, J.J. and Weisberg, P.J. 1995 Using aerial photography and GIS to map the forest-tundra ecotone in Rocky Mountain National Park, Colorado, for global change research. *Photogramm. Eng. Remote Sens.* **61**, 313–320.

Bauer, M.E., Burk, T.E., Ek, A.R., Coppin, P.R., Lime, S.D., Walsh, T.A. *et al*. 1994 Satellite inventory of Minnesota forest resources. *Photogramm. Eng. Remote Sens.* **60**, 287–298.

Baumann, M., Ozdogan, M., Kuemmerle, T., Wendland, K.J., Esipova, E. and Radeloff, V.C. 2012 Using the Landsat record to detect forest-cover changes during and after the collapse of the Soviet Union in the temperate zone of European Russia. *Remote Sens. Environ.* **124**, 174–184.

Bühler, Y., Marty, M. and Ginzler, C. 2012 High resolution DEM generation in high-alpine terrain using airborne remote sensing techniques. *Transact. GIS.* **16**, 635–647.

Choi, O. and Kweon, I.S. 2009 Robust feature point matching by preserving local geometric consistency. *Comput. Vis. Image Underst.* **113**, 726–742.

Coppin, P., Jonckheere, I., Nackaerts, K., Muys, B. and Lambin, E. 2004 Review ArticleDigital change detection methods in ecosystem monitoring: a review. *Int. J. Remote Sens.* **25**, 1565–1596.

Dai, X.L. and Khorram, S. 1999 Remotely sensed change detection based on artificial neural networks. *Photogramm. Eng. Remote Sens.* **65**, 1187–1194.

Desclée, B., Bogaert, P. and Defourny, P. 2006 Forest change detection by statistical object-based method. *Remote Sens. Environ.* **102**, 1–11.

Elhadi, E.M. and Zomrawi, N. 2009 Object-based land use/cover extraction from QuickBird image using Decision tree. *Nature Sci.* **7**, 32–36.

Fraser, R.H., Abuelgasim, A. and Latifovic, R. 2005 A method for detecting large-scale forest cover change using coarse spatial resolution imagery. *Remote Sens. Environ.* **95**, 414–427.

Ginzler, C. and Hobi, M.L. 2015 Countrywide stereo-image matching for updating digital surface models in the framework of the swiss national forest inventory. *Remote Sens.* **7**, 4343–4370.

Haala, N. 2009 Comeback of digital image matching. *Photogramm. Week.* **2009**, 289–301.

Hansen, M.C., Potapov, P.V., Moore, R., Hancher, M., Turubanova, S.A., Tyukavina, A. *et al*. 2013 High-resolution global maps of 21st-century forest cover change. *Science.* **342**, 850–853.

Hayes, D.J. and Cohen, W.B. 2007 Spatial, spectral and temporal patterns of tropical forest cover change as observed with multiple scales of optical satellite data. *Remote Sens. Environ.* **106**, 1–16.

Hirschmüller, H. 2008 Stereo processing by semiglobal matching and mutual information. *IEEE Transact. Pattern Anal. Mach. Intell.* **30**, 328–341.

Hobi, M.L. and Ginzler, C. 2012 Accuracy assessment of digital surface models based on WorldView-2 and ADS80 stereo remote sensing data. *Sensors.* **12**, 6347–6368.

Hussain, M., Chen, D., Cheng, A., Wei, H. and Stanley, D. 2013 Change detection from remotely sensed images: from pixel-based to object-based approaches. *ISPRS J. Photogramm. Remote Sens.* **80**, 91–106.

Lawrence, M., McRoberts, R.E., Tomppo, E., Thomas, G. and Karl, G. 2010 *National Forest Inventories - Pathways for Common Reporting*. Tomppo, E., Gschwantner, T., Lawrence, M. and McRoberts, R.E. (eds). Springer, pp. 24–26.

Lu, D., Mausel, P., Brondízio, E. and Moran, E. 2004 Change detection techniques. *Int. J. Remote Sens.* **25**, 2365–2401.

Maltamo, M., Naesset, E. and Vauhkonen, J. 2014 Forestry applications of airborne laser scanning: concepts and case studies. In *Managing Forest Ecosystems*. Springer.

Mas, J.F. 1999 Monitoring land-cover changes: a comparison of change detection techniques. *Int. J. Remote Sens.* **20**, 139–152.

McRoberts, R.E. and Tomppo, E.O. 2007 Remote sensing support for national forest inventories. *Remote Sens. Environ.* **110**, 412–419.

Mortensen, E.N., Hongli, D. and Shapiro, L. 2005 A SIFT descriptor with global context. In *Computer Vision and Pattern Recognition, 2005. CVPR 2005. IEEE Computer Society Conference on*, pp. 184–190 vol. 181.

Olofsson, P., Foody, G.M., Herold, M., Stehman, S.V., Woodcock, C.E. and Wulder, M.A. 2014 Good practices for estimating area and assessing accuracy of land change. *Remote Sens. Environ.* **148**, 42–57.

Paine, D.P. and Kiser, J.D. 2003 *Aerial Photography and Image Interpretation*. Wiley.

Poon, J., Fraser, C.S., Chunsun, Z., Li, Z. and Gruen, A. 2005 Quality assessment of digital surface models generated from IKONOS imagery. *Photogramm. Rec.* **20**, 162–171.

Sandau, R., Braunecker, B., Driescher, H., Eckardt, A., Hilbbert, S., Hutton, J. *et al*. 2000 Design principles of the LH Systems ADS40 airborne digital sensor. *Int. Arch. Photogramm. Remote Sens.* **33** (Part B1), 258–265.

Singh, A. 1989 Review article digital change detection techniques using remotely-sensed data. *Int. J. Remote Sens.* **10**, 989–1003.

Skowronski, N.S., Clark, K.L., Gallagher, M., Birdsey, R.A. and Hom, J.L. 2014 Airborne laser scanner-assisted estimation of aboveground biomass change in a temperate oak–pine forest. *Remote Sens. Environ.* **151**, 166–174.

Song, X.-P., Huang, C., Sexton, J., Channan, S. and Townshend, J. 2014 Annual detection of forest cover loss using time series satellite measurements of percent tree cover. *Remote Sens.* **6**, 8878–8903.

Spurr, S.H. 1960 *Photogrammetry and Photo-interpretation*. 2nd edn. The Ronald Press Company.

Straub, C., Stepper, C., Seitz, R. and Waser, L.T. 2013 Potential of UltraCamX stereo images for estimating timber volume and basal area at the plot level in mixed European forests. *Can. J. For. Res.* **43**, 731–741.

swisstopo. 2015 *SWISSIMAGE*. http://www.swisstopo.admin.ch/internet/swisstopo/de/home/products/images/ortho/swissimage.html (accessed on 08 April, 2015).

Tack, F., Goossens, R. and Buyuksalih, G. 2012 Assessment of a photogrammetric approach for urban DSM extraction from tri-stereoscopic satellite imagery. *Photogramm. Rec.* **27**, 293–310.

Tian, J., Reinartz, P., d'Angelo, P. and Ehlers, M. 2013 Region-based automatic building and forest change detection on Cartosat-1 stereo imagery. *ISPRS J. Photogramm. Remote Sens.* **79**, 226–239.

Waser, L.T., Baltsavias, E., Ecker, K., Eisenbeiss, H., Feldmeyer-Christe, E., Ginzler, C. *et al*. 2008 Assessing changes of forest area and shrub encroachment in a mire ecosystem using digital surface models and CIR aerial images. *Remote Sens. Environ.* **112**, 1956–1968.

Waser, L.T., Ginzler, C., Kuechler, M., Baltsavias, E. and Hurni, L. 2011 Semi-automatic classification of tree species in different forest ecosystems by spectral and geometric variables derived from Airborne Digital Sensor (ADS40) and RC30 data. *Remote Sens. Environ.* **115**, 76–85.

White, J., Wulder, M., Vastaranta, M., Coops, N., Pitt, D. and Woods, M. 2013 The utility of image-based point clouds for forest inventory: a comparison with airborne laser scanning. *Forests.* **4**, 518–536.

Wulder, M.A., Han, T., White, J.C., Sweda, T. and Tsuzuki, H. 2007 Integrating profiling LIDAR with Landsat data for regional boreal forest canopy attribute estimation and change characterization. *Remote Sens. Environ.* **110**, 123–137.

Wulder, M.A., Butson, C.R. and White, J.C. 2008 Cross-sensor change detection over a forested landscape: options to enable continuity of medium spatial resolution measures. *Remote Sens. Environ.* **112**, 796–809.

Zhang, L. and Gruen, A. 2006 Multi-image matching for DSM generation from IKONOS imagery. *ISPRS J. Photogramm. Remote Sens.* **60**, 195–211.

Zhang, B., Miller, S., Walker, S. and DeVenencia, K. 2007 Next Generation Automatic Terrain Extraction using Microsoft UltraCam imagery. In *Proceedings of the ASPRS 2007 Annual Conference*, Tampa.